JOURNAL OF NATURAL PRODUCTS

Article

Cite This: J. Nat. Prod. XXXX, XXX, XXX−XXX

pubs.acs.org/jnp

Triterpenoids from *Ganoderma gibbosum*: A Class of Sensitizers of FLC-Resistant *Candida albicans* to Fluconazole

Debing Pu,[†,§,⊥] Xiaoning Li,[‡,⊥] Jing Lin,[†] Ruihan Zhang,[†] Ting Luo,[†] Yuan Wang,[†] Junbo Gao,[†] Muhammad Aurang Zeb,[†] Xingjie Zhang,[†] Xiaoli Li,[*,†] Ruirui Wang,[*,‡] and Weilie Xiao[*,†,§]

[†]Key Laboratory of Medicinal Chemistry for Natural Resource of Ministry of Education and Yunnan Province, School of Chemical Science and Technology, Yunnan University, Kunming 650091, People's Republic of China

[‡]School of Pharmaceutical Sciences, Yunnan University of Chinese Medicine, Kunming 650500, People's Republic of China

[§]State Key Laboratory for Conservation and Utilization of Bio-Resources in Yunnan, Center for Life Sciences, School of Life Sciences, Yunnan University, Kunming 650091, People's Republic of China

Supporting Information

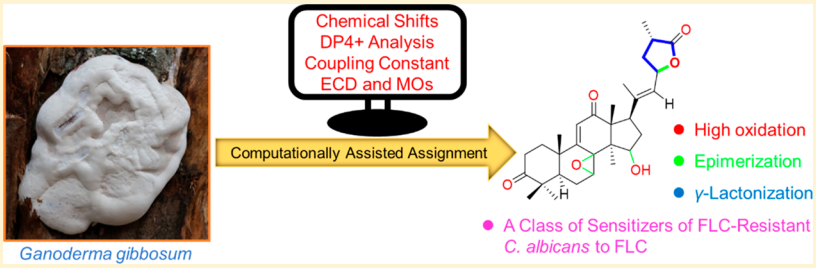

ABSTRACT: Fungal drug resistance is a major health threat, and reports of clinical resistance worldwide are becoming increasingly common. In a research program to discover new molecules to help overcome this problem, 14 new lanostane-type triterpenoids, gibbosicolids A−G (**2**−**8**) and gibbosic acids I−O (**9**−**15**), were isolated from the fruiting bodies of *Ganoderma gibbosum*, along with seven known triterpenoid derivatives. These compounds featured high levels of oxidation, epimerization, and γ-lactonization. Structures were elucidated by comprehensive spectroscopic analyses and HRMS data. Absolute configurations were assigned based on quantum chemical calculations, including calculated chemical shift with DP4+ analysis, coupling constants, and electronic circular dichroism (ECD) methods. Results show that the calculated NMR with DP4+ analysis could not reliably establish the overall spatial configuration of molecules possessing independent and free-rotational stereoclusters. All these compounds significantly increased the sensitivity of fluconazole (FLC)-resistant *C. albicans* to FLC. Compounds **2**, **5**, **9**, **12**, **16**, **17**, and **21** exhibited strong antifungal activity against FLC-resistant *C. albicans* when combined with FLC, with MIC_{50} values ranging from 3.8 to 8.8 μg/mL.

Candida albicans is an opportunistic fungus, which has been reported to be one of the most common nosocomial infectious fungal species. It is a commensal organism that exists in the healthy human urogenital and gastrointestinal tracts.[1] *C. albicans* can also induce disseminated candidiasis and can cause a high rate of morbidity and mortality of 40−60%, especially in immunocompromised patients, such as those with AIDS or neutropenia.[2] Fluconazole (FLC) is a commonly used antifungal drug due to its low toxicity, easy oral administration, and high bioavailability.[3] However, due to the intensive long-term application of antifungal drugs, the level of drug resistance reported in the health sector has dramatically increased in recent years.[4] Therefore, it is essential that new treatments are explored for the prevention of infections by drug-resistant strains of *C. albicans*. Natural products from traditional Chinese herbs are structurally diverse and exert a variety of pharmacological activities in clinical use. Combination therapy approaches, using both antifungal drugs and natural products, have been assessed and were found to be a promising treatment method.[5]

The fruiting bodies of *Ganoderma*, especially *G. lucidum* and *G. applanatum*, are important Traditional Chinese Medicine materials, which are used for the promotion of longevity and maintenance of vitality. Numerous lanostane-type triterpenic acids have been isolated and identified as principal active constituents.[6] Due to their wide range of bioactivities, these compounds have attracted much attention from pharmaceutical chemists and phytochemists.[7] However, it is still difficult to fully establish the stereochemistry of oxidized side chains in these structures.[8] In the present study, 21 highly oxygenated lanostane-type triterpenoids (Chart 1), including 14 new compounds (**2**−**15**), were isolated from the fruiting bodies of *G. gibbosum*. The stereochemistry of these compounds was comprehensively established via quantum chemical calcula-

Received: February 15, 2019

DOI: 10.1021/acs.jnatprod.9b00148
J. Nat. Prod. XXXX, XXX, XXX−XXX

Chart 1

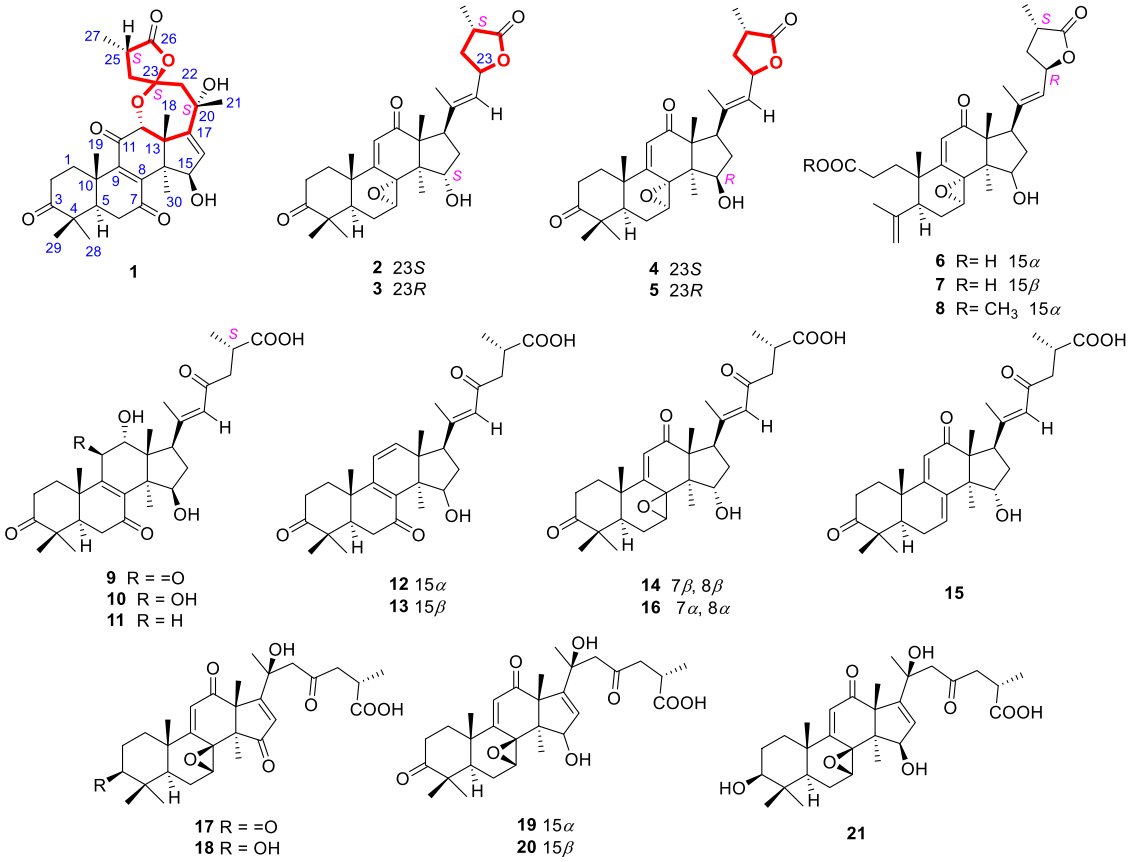

tions, including computational NMR with DP4+ analysis,[9] coupling constants, and electronic circular dichroism (ECD) methods. Bioactivity experiments were performed to assess antifungal activity of the identified compounds against standard *C. albicans* and FLC-resistant *C. albicans*. The antifungal activities of the compounds were assessed both alone and in combination with FLC.

RESULTS AND DISCUSSION

The known compound ganoapplanilactone A (**1**) was reported recently and contains a rare spiro-lactone segment.[10] Although the absolute configuration of this compound was assigned by comparing calculated and experimental ECD data, not all candidate configurations were taken into account when calculating ECD. The stereochemistry of austrolactone, the first reported analogue possessing a spiro-lactone moiety with a 7/5-ring system, has also not been clearly described.[11] All possible candidate configurations of **1** were considered, and its absolute configuration was established by a combination of computational NMR with DP4+ analysis and ECD methods. The planar structure and partial relative configuration of compound **1** were established based on correlations of ^{1}H−^{1}H COSY, HMBC, and ROESY spectra (Figure 1a and b). Due to the lack of spectroscopic relationships observed, it was not possible to establish the relative configurations of C-23 and C-25 in the spiro-lactone segment using ROESY correlation analysis. This suggests (in terms of the whole-compound stereochemistry) that there were four relative configurations reasonably possible: 23*S**,25*S**-**1** (**1a**); 23*R**,25*S**-**1** (**1b**); 23*R**,25*R**-**1** (**1c**); 23*S**,25*R**-**1** (**1d**).

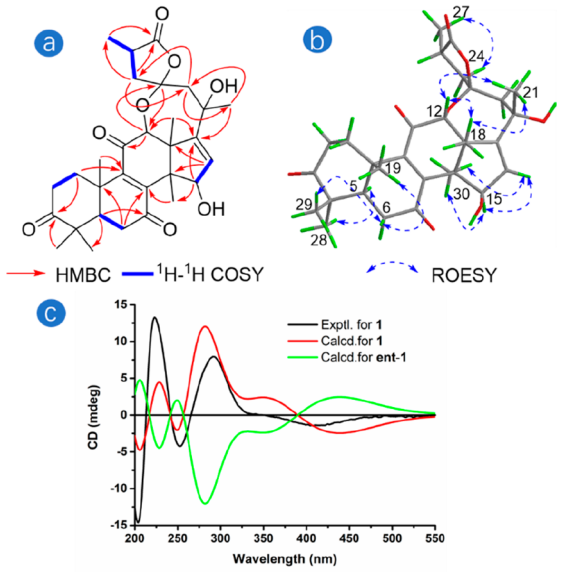

Figure 1. Important HMBC and ^{1}H−^{1}H COSY correlations (a); ROESY correlations (b); and ECD spectra (c) of compound **1**.

Calculated NMR with DP4+ analysis[9] was employed to establish the relative configuration of the compound from the four possibilities. Chemical shifts of isomers **1a**, **1b**, **1c**, and **1d** were predicted using the gauge-independent atomic orbital (GIAO) method,[12] with density functional theory (DFT) calculations in chloroform, using the polarizable continuum model (PCM) model at the mPW1PW91/6-311G(d,p)//B3LYP/6-31+G(d,p) level. Next, the experimental and

DOI: 10.1021/acs.jnatprod.9b00148
J. Nat. Prod. XXXX, XXX, XXX−XXX

Table 1. ^{1}H NMR Data for Compounds 2−8 Measured at 600 MHz (δ in ppm, J in Hz)[a]

position	2	3	4	5	6	7	8
1a	2.11, m	2.13, overlap	2.10, overlap	2.10, overlap	2.13, overlap	2.16, overlap	2.14, overlap
1b	1.94, ddd (13.6,9.2,4.8)	1.96, ddd, (13.6, 9.2,4.7)	1.99, ddd (13.5,8.8,4.9)	1.99, ddd (13.6, 8.9,4.9)	1.85, overlap	1.83, overlap	1.83, overlap
2a	2.66, overlap	2.70, overlap	2,64, overlap	2.65, m	2.43, m	2.40, overlap	2.38, m
2b	2.7, m	2.50, m	2.47, overlap	2.49, overlap	2.22, dt (10.6, 5.5)	2.19, overlap	2.20, overlap
5	2.75, dd (12.7, 2.5)	2.78, dd (12.7, 2.4)	2.71, dd (12.7, 2.8)	2.74, overlap	2.90, dd (12.8, 3.2)	2.89, dd (12.6, 3.1)	2.90, dd (12.8, 3.4)
6a	2.17, m	2.19, m	2.07, overlap	2.08, overlap	2.14, overlap	2.02, dd (10.8, 3.8)	2.16, overlap
6b	1.82, dd (14.3, 13.2)	1.83, overlap	1.85, overlap	1.83, overlap	1.92, overlap	1.90, d (12.0)	1.90, overlap
7	4.12, d (3.6)	4.14, d (3.5)	4.74, d (3.8)	4.75, d (3.7)	4.06, d (3.9)	4.80, d (4.0)	4.05, d (4.0)
11	6.04, s	6.06, s	6.05, s	6.05, s	5.97, s	5.98, s	5.96, s
15	4.42, t (8.5)	4.42, t (8.4)	3.98, d (3.2)	3.99, d (2.9)	4.38, t (8.4)	4.01, d (6.0)	4.37, t (8.4)
16a	2.35, m	2.35, m	2.46, overlap	2.47, overlap	2.31, m	2.47, m	2.29, m
16b	1.76, ddd (14.4, 11.5, 7.9)	1.79, overlap	1.81, overlap	1.81, overlap	1.83, overlap	1.77, overlap	1.80, overlap
17	3.23, dd (11.3, 7.9)	3.27, dd (11.1, 7.0)	3.21, dd (10.6, 7.4)	3.18, dd (10.8, 7.2 Hz)	3.20, dd (11.0, 7.3)	3.06, dd (9.6, 8.6)	3.20, dd (11.2, 7.2)
18	0.99, s	0.99, s	1.24, s	1.21, s	0.97, s	1.23, s	0.98, overlap
19	1.09, s	1.10, s	1.11, s	1.10, s	1.00, s	1.00, overlap	0.99, overlap
21	1.88, s	1.89, s	1.89, s	1.91, s	1.90, s	1.94, s	1.90, s
22	5.44, d (8.1)	5.55, d (8.0)	5.52, d (8.0)	5.57, d (8.0)	5.54, d (7.9)	5.57, d (8.0)	5.54, d (7.9)
23	5.12, ddd (10.3, 8.1, 5.7)	5.31, dd (13.2, 8.0)	5.14, ddd (10.2, 8.0, 5.8)	5.32, dd (13.0, 8.0	5.30, dd (13.3, 7.9)	5.33, dd (12.9, 8.0)	5.29, dd (13.2, 7.9)
24a	2.55, ddd (13.1, 9.4,5.7)	2.13, overlap	2.55, ddd (13.6, 8.3, 5.8)	2.10, overlap	2.15, overlap	2.13, overlap	2.12, overlap
24b	1.64, dd (23.0, 10.3)	2.13, overlap	1.63, dd (23.0, 10.2)	2.10, overlap	2.15, overlap	2.13, overlap	2.12, overlap
25	2.66, overlap	2.73, overlap	2.66, overlap	2.73, overlap	2.7, m	2.75, m	2.72, dt (15.3, 7.3)
27	1.29, d (7.0)	1.32, d (7.3)	1.28, d (7.0)	1.29, d (7.3)	1.30, d (7.3)	1.29, d (7.3)	1.3, d (7.3)
28a	1.12, s	1.14, s	1.13, s	1.12, s	4.96, s	4.94, s	4.96, s
28b					4.75, s	4.74, s	4.75, s
29	1.10, s	1.13, s	1.08, s	1.08, s	1.75, s	1.74, s	1.75, s
30	1.16, s	1.19, s	1.00, s	1.00, s	1.17, s	1.00, overlap	1.17, s
3-OCH_3							3.66, s

[a]In chloroform-*d*.

calculated chemical shifts were statistically analyzed based on DP4+ probability. DP4+ analysis results show that isomer **1a** (Table S1-1 and Figure S25-1) is the most reasonable configuration, with a probability of 100% for the combination of ^{1}H and ^{13}C data. Isomer 23*S*,25*S*-**1** and its enantiomer (**ent-1**) were selected to establish their absolute configuration by fitting to calculated and experimental ECD curves. The time-dependent density functional theory (TDDFT) method[13] at the B3LYP/6-311+G(d,p)//B3LYP/6-31+G(d,p) level in methanol was used with the PCM model to simulate the ECD spectra. Results show that the calculated curve for **1** was consistent with the experimental spectrum, while the opposite was observed for that of its enantiomer (Figure 1c). Therefore, the absolute configurations of C-23 and C-25 in this compound were established as 23*S* and 25*S* (Chart 1).

The molecular formulas of **2** and **3** were determined as $C_{30}H_{40}O_6$ by HRESIMS of their pseudomolecular ions. NMR data analysis (Tables 1 and 2) suggested the two compounds were lanostane-type triterpenoid derivatives. The NMR signals of these two lanostane-type triterpenoid derivatives were almost identical, except for the coupling constants at H-23 (ddd, J = 10.3, 8.1, 5.7 Hz for **2**; dd, J = 13.2, 8.0 Hz for **3**). These findings suggest that the two compounds could be a pair of epimers with different configurations at C-23. The structures, including partial relative configurations, were initially elucidated through comparison of their chemical shifts with that of australic acid,[11] along with analyses of 2D NMR correlations (Figure 2) and HRESIMS data. However, the relative configurations of the γ-lactone group could not be convincingly assigned from the weak correlations between H-23/H-25 in compound **2** and H-23/H-27 in compound **3**. In consideration of the different coupling constants at H-23, calculated coupling constants were employed to distinguish the two. Calculations of the spin−spin interactions of the two possible relative configurations (23*S**/25*S** and 23*R**/25*S**) were performed at the mPW1PW91/6-311G(d,p)//B3LYP/6-31+G(d,p) level in chloroform, using the PCM model. Results show that the predicted coupling constant for 23*S**/25*S** (J = 8.7, 7.7, 5.0 Hz) was close to that of compound **2**, with a ddd peak type, while the calculated constant for 23*R**/25*S** (J = 8.6, 8.1, 0.5 Hz) was similar to that of compound **3**, with a peak type of dd (Figure 3). Based on this analysis of coupling constants, their relative configurations at the lactone group were assigned as 23*S**/25*S** for compound **2** and 23*R**/25*S** for compound **3**.

The results of the ECD experiment (Figure 4) clearly show that the Cotton effects (CEs) of these compounds at 200 and 210 nm were opposite, suggesting that the different

DOI: 10.1021/acs.jnatprod.9b00148
J. Nat. Prod. XXXX, XXX, XXX−XXX

Table 2. ^{13}C NMR Data for Compounds 2−15 (δ in ppm)

position	2[a]	3[a]	4[a]	5[a]	6[a]	7[a]	8[a]	9[a]	10[b]	11[a]	12[a]	13[a]	14[c]	15[c]
1	35.9, t	35.9, t	36.2, t	36.1, t	36.1, t	36.1, t	36.4, t	34.9, t	34.1, t	35.3, t	35.3, t	35.6, t	37.4, t	36.2, t
2	33.5, t	33.6, t	33.7, t	33.7, t	29.2, t	29.3, t	29.4, t	33.9, t	34.6, t	34.2, t	33.9, t	34.0, t	34.2, t	35.0, t
3	216.2, s	216.3, s	216.6, s	216.6, s	178.4, s	178.8, s	173.9, s	215.2, s	213.9, s	213.8, s	214.5, s	214.4, s	213.4, s	214.4, s
4	45.9, s	45.8, s	45.9, s	45.9, s	144.1, s	144.6, s	144.2, s	46.4, s	47.4, s	47.3, s	46.7, s	46.9, s	47.7, s	47.7, s
5	40.7, d	40.7, d	40.4, d	40.4, d	44.0, d	43.7, d	43.9, d	49.6, d	51.5, d	49.8, d	49.2, d	49.3, d	49.9, d	50.3, d
6	23.2, t	23.1, t	23.1, t	23.1, t	27.2, t	27.3, t	27.3, t	37.3, t	37.6, t	37.1, t	36.4, t	36.7, t	22.0, t	24.4, t
7	60.5, d	60.5, d	62.9, d	62.8, d	61.3, d	63.4, d	61.3, d	203.6, s	202.6, s	201.1, s	201, s	201.5, s	57.8, d	131.7, d
8	66.7, s	66.6, s	64.2, s	64.2, s	67.4, s	66.1, s	67.4, s	151.7, s	138.6, s	138.5, s	135.8, s	134.9, s	62.4, s	141.2, s
9	162.8, s	163.0, s	164.3, s	164.5, s	162.0, s	163.5, s	162.0, s	150.4, s	165.1, s	165.8, s	159.1, s	160.7, s	162.9, s	161.9, s
10	40.1, s	40.1, s	40.1, s	40.1, s	43.5, s	43.6, s	43.6, s	39.0, s	40.4, s	39.6, s	37.9, s	38.0, s	37.9, s	38.7, s
11	131.1, d	131.0, d	130.3, d	130.3, d	130.4, d	129.9, d	130.4, d	203.9, s	77.4, d	36.2, t	122.7, d	122.0, d	126.9, d	119.1, d
12	201.6, s	201.5, s	203.1, s	203.0, s	201.4, s	203.0, s	201.3, s	79.2, d	80.5, d	70.8, d	146.5, d	147.6, d	203.1, s	203.6, s
13	58.9, s	58.8, s	59.4, s	59.4, s	58.9, s	59.3, s	58.9, s	52.9, s	49.5, s	50.8, s	51.0, s	50.2, s	58.3, s	58.8, s
14	50.4, s	50.4, s	53.4, s	53.3, s	50.9, s	53.3, s	50.9, s	49.8, s	53.4, s	51.9, s	51.4, s	52.5, s	50.5, s	53.5, s
15	71.6, d	71.6, d	76.5, d	76.4, d	71.0, d	77.0, d	71.0, d	77.4, d	78.4, d	78.3, d	70.6, d	75.0, d	69.2, d	73.0, d
16	33.5, t	33.5, t	39.6, t	39.8, t	33.3, t	39.9, t	33.3, t	33.8, t	35.8, t	34.9, t	32.9, t	36.1, t	35.8, t	37.6, t
17	43.9, d	44.0, d	46.0, d	46.0, d	44.4, d	46.2, d	44.4, d	46.8, d	33.8, t	46.7, d	47.1, d	48.6, d	47.0, d	46.9, d
18	18.1, q	18.1, q	19.6, q	19.8, q	17.8, q	19.4, q	17.8, q	18.5, q	19.1, q	18.0, q	16.3, q	17.1, q	18.7, q	22.7, q
19	24.5, q	24.5, q	24.8, q	24.8, q	23.1, q	23.3, q	23.2, q	18.2, q	18.3, q	17.7, q	19.4, q	19.5, q	20.9, q	21.8, q
20	141.5, s	140.5, s	141.7, s	140.9, s	140.6, s	140.9, s	140.6, s	157.8, s	159.0, s	159.3, s	157.9, s	157.7, s	157.3, s	158.4, s
21	18.7, q	18.8, q	18.6, q	19.2, q	19.0, q	19.1, q	19.0, q	20.4, q	20.6, q	21.0, q	21.2, q	21.5, q	21.2, q	21.7, q
22	125.6, d	126.0, d	126.0, d	126.0, d	126.1, d	126.1, d	126.1, d	124.8, d	125.1, d	124.4, d	124.4, d	124.7, d	126.0, d	126.9, d
23	75.3, d	75.3, d	75.5, d	75.7, d	75.4, d	75.8, d	75.3, d	198.6, s	199.1, s	198.9, s	198.3, s	198.4, s	199.2, s	199.7, s
24	38.0, t	37.1, t	38.0, t	37.2, t	37.1, t	37.2, t	37.1, t	47.4, t	48.5, t	47.5, t	47.5, t	47.5, t	48.5, t	48.9, t
25	36.0, d	34.3, d	36.0, d	34.4, d	34.4, d	34.4, d	34.3, d	34.7, d	36.0, d	34.8, d	34.6, d	34.7, d	35.7, d	36.3, d
26	179.6, s	180.0, s	179.7, s	180.2, s	180.1, s	180.4, s	180, s	180.4, s	178.8, s	179.6, s	180.1, s	180.4, s	178.0, s	178.4, s
27	15.0, q	15.7, q	15.0, q	15.7, q	15.7, q	15.7, q	15.7, q	16.9, q	17.7, q	17.0, q	17.0, q	17.0, q	17.7, q	18.2, q
28	28.7, q	28.6, q	28.5, q	28.5, q	115.8, q	115.6, q	115.8, q	26.9, q	25.0, q	25.1, q	26.1, q	25.5, q	24.7, q	25.9, q
29	21.6, q	21.6, q	21.7, q	21.7, q	23.2, q	23.6, q	23.3, q	20.4, q	21.5, q	21.4, q	20.7, q	20.6, q	21.9, q	18.7, q
30	14.6, q	14.5, q	21.1, q	21.0, q	14.6, q	20.9, q	14.6, q	27.4, q	26.5, q	24.9, q	15.1, q	20.9, q	16.4, q	19.4, q
$-OCH_3$							51.7							

[a]Measured at 150 MHz in chloroform-*d*. [b]Measured at 150 MHz in pyridine-d_5. [c]Measured at 200 MHz in pyridine-d_5.

DOI: 10.1021/acs.jnatprod.9b00148
J. Nat. Prod. XXXX, XXX, XXX−XXX

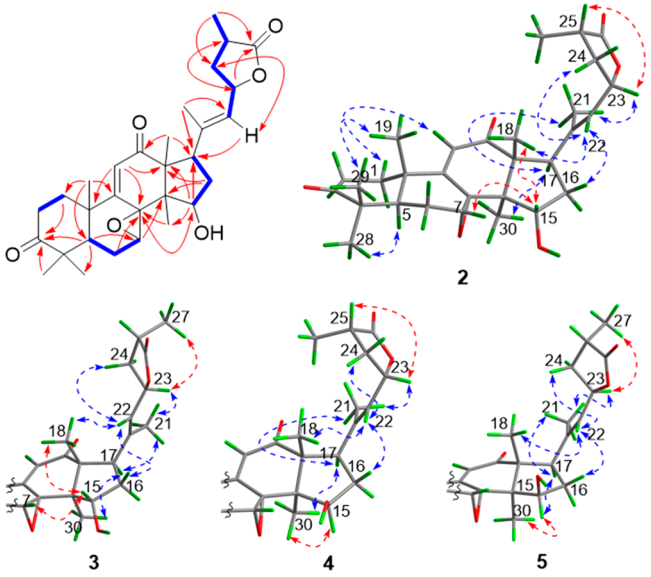

Figure 2. Important HMBC (solid arrow), ^{1}H−^{1}H COSY (bold), and ROESY (dashed double arrow) correlations for compounds **2**−**5**.

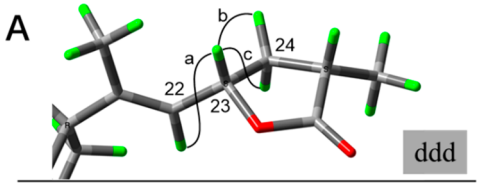

Configuration	H-H	*J* (Hz)	Dihedral angle
23*S**/ 25*S**	a	7.7	-151 °
	b	5.0	-40 °
	c	8.7	-152 °

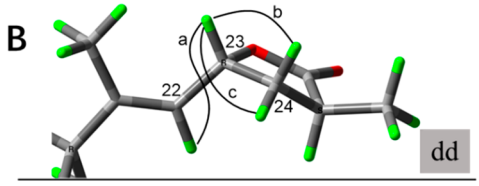

Configuration	H-H	*J* (Hz)	Dihedral angle
23*R**/ 25*S**	a	8.6	132 °
	b	8.1	-23 °
	c	0.5	96°

Figure 3. Calculated results of coupling constants and dihedral angles for 23*S**,25*S**-**2** (A) and 23*R**,25*S**-**3** (B).

configurations at C-23 may lead to the differences in their ECD curves. To correctly identify the absolute configuration of compounds **2** and **3**, the predicted ECD curves for four possible configurations (23*S*/25*S*-**2**; 23*R*/25*R*-**2**; 23*R*/25*S*-**3**; and 23*S*/25*R*-**3**) were calculated at the B3LYP/6-311+G-(d,p)//B3LYP/6-31+G(d,p) level in methanol, using the PCM model. Results show that the predicted curve for 23*S*/25*S*-**2** closely coincided with the experimentally generated curve for **2**, but differed from that of 23*R*/25*R*-**2** (Figure 4). Similarly, the computational ECD curve generated for 23*R*/25*S*-**3** closely corresponded with the experimentally generated curve for **3** (Figure 4). The molecular orbitals (MOs) analysis of the

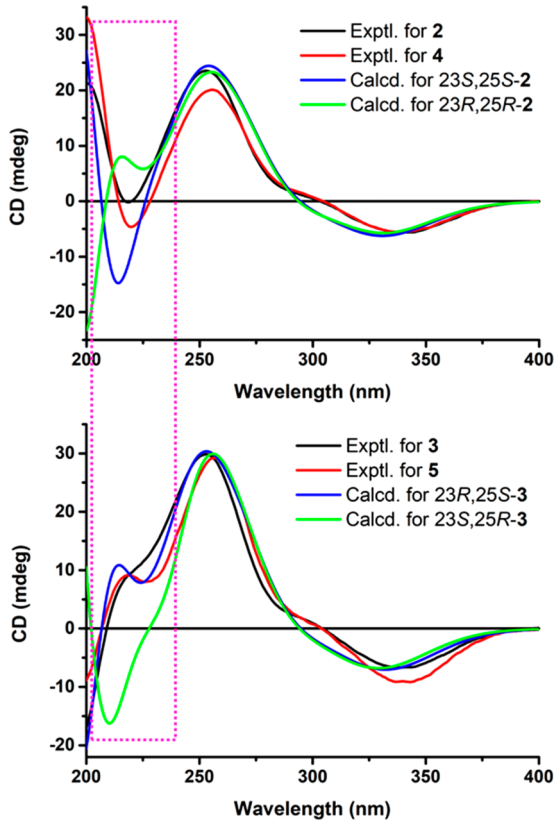

Figure 4. Experimental and calculated ECD spectra for compounds **2**−**5**.

lowest energy conformer 23*S*/25*S*-**2**-**1** (70%) (Figure 5A and Table S27-1) revealed that the negative CE at 210 nm observed in the experimental curve of **2** could be attributed to a $\pi \rightarrow \pi^*$ electronic transition on the side chain, from MO 134 to MO 137. Furthermore, the positive CE at 200 nm could be assigned to another $\pi \rightarrow \pi^*$ transition from MO 129 to MO 137. Similarly, analysis of the MOs of 23*R*/25*S*-**3**-**2** (37%) (Figure 5B and Table S27−1) showed that the positive curve of compound **3** at 207 nm could be attributed to a $\pi \rightarrow \pi^*$ transition from MO 134 to MO 137, while the negative CE at 201 nm could be assigned to another $\pi \rightarrow \pi^*$ electronic transition from MO 129 to MO 137. Therefore, the configurations were identified as 23*S*/25*S* for compound **2** and 23*R*/25*S* for compound **3**. The structures were established as (23*S*, 25*S*)-15α-hydroxy-7α,8α-epoxy-3,12-dioxolanosta-9-(11),20*E*(22)-dien-23,26-olide (named gibbosicolid A) (**2**) and (23*R*, 25*S*)-15α-hydroxy-7α,8α-epoxy-3,12-dioxolanosta-9(11),20*E*(22)-dien-23,26-olide (named gibbosicolid B) (**3**).

Similarly, compounds **4** and **5** were also determined to be a pair of epimers with differing configurations at C-23, based on HRESIMS and NMR data. The structures of **4** and **5** were similar to compounds **2** and **3**, except for a subtle difference of chemical signals [$\delta_{H\text{-}15}$ 3.98 (1H, d, *J* = 3.2 Hz), $\delta_{C\text{-}15}$ 76.5 for **4** and **5** (Tables 1 and 2), while $\delta_{H\text{-}15}$ 4.42 (1H, t, *J* = 8.5 Hz), $\delta_{C\text{-}15}$ 71.6 for **2** and **3**]. These findings indicate that in compounds **4** and **5** the configurations of OH-15 were in the β-orientation, with their planar structure and partial relative configurations confirmed by the correlation between ^{1}H−^{1}H COSY, HMBC, and ROESY spectra (Figure 2). The absolute configurations of compounds **4** and **5** were also identified as 23*S*/25*S* for **4** and 23*R*/25*S* for **5** by comparing their

DOI: 10.1021/acs.jnatprod.9b00148
J. Nat. Prod. XXXX, XXX, XXX−XXX

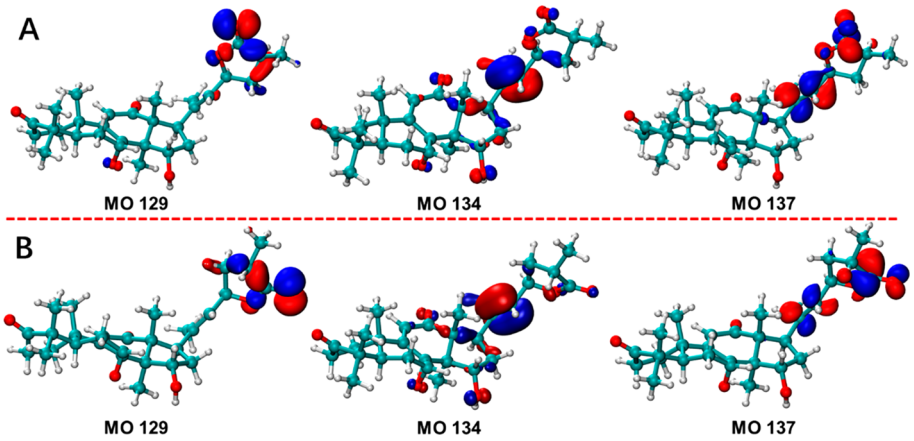

Figure 5. Key MOs involved in important transitions of conformers **2**-**1** (A) and **3**-**2** (B).

experimental ECD curves with those of compounds **2** and **3**, respectively (Figure 4). Therefore, the structures of compounds **4** and **5** were established as shown in Chart 1 and named gibbosicolids C and D (**4** and **5**).

Compounds **6** and **7** were also considered to be a pair of epimers with differing configurations at C-15, based on NMR and HRESIMS data. The OH-15 configurations of compounds **6** and **7** were elucidated as being in the α-orientation for **6** and the β-orientation for **7**, based on ROESY correlation analysis (Figures S2-1 and S2-2) and comparison of chemical shifts with those of compounds **2**−**5**. However, in contrast to **2**−**5**, compounds **6** and **7** have an exocyclic double bond and a carboxyl group. By comprehensive analysis of the correlations of HMBC and ^{1}H−^{1}H COSY (Figures S2-1 and S2-2), the carboxyl group was located at C-3 and the position of the double bond was assigned between C-4 and C-28, indicating that ring A in these structures was subjected to an oxidative cleavage, like the known compound elfvingic acid H.[14] The planar structure of compounds **6** and **7** and their relative configurations were confirmed by analysis of their 2DNMR correlations (Figures S2-1 and S2-2) and comparison of their NMR data with those of compounds **2**, **3**, and elfvingic acid H. The calculated ECD method assigned their absolute configurations as 23*R*,25*S* (Figure 6). Therefore, the structures were determined to be (23*R*,25*S*)-15α-hydroxyl-7α,8α-epoxy-12-oxo-3,4-seco-lanosta-4(28),9(11),20*E*(22)-trien-23,26-olide-3-oic acid (named gibbosicolid E) (**6**) and (23*R*,25*S*)-15β-hydroxyl-7α,8α-epoxy-12-oxo-3,4-seco-lanosta-4(28),9(11),20*E*(22)-trien-23,26-olide-3-oic acid (named gibbosicolid F) (**7**).

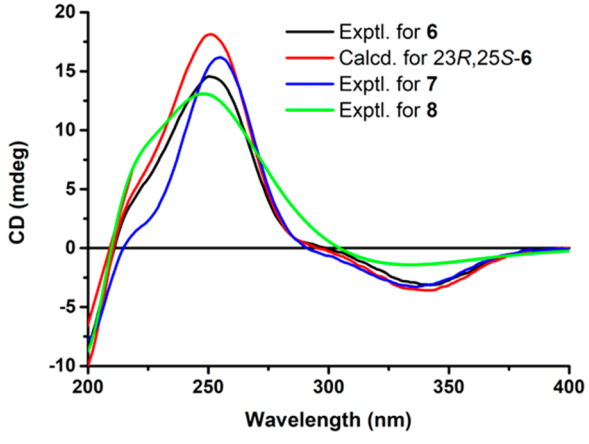

Figure 6. Experimental and calculated ECD spectra for compounds **6**−**8**.

Based on analysis of HRESIMS and NMR data, compound **8** was identified as a methylated product of compound **6**. The HMBC correlation (Figure S2-3) of the methyl (C$\underline{H}_3$) with carboxyl (−$\underline{C}$OOH) groups at C-3 strongly implied that the methyl group was linked to the carboxyl group. The other fragments of compound **8** were identical to those of compound **6**, according to both 2D NMR and ECD analyses (Figure 6). Therefore, the structure was identified as shown (named gibbosicolid G).

HRMS data established the molecular formula of compound **9** as $C_{30}H_{40}O_8$, with 11 indices of hydrogen deficiency. Based on NMR data analysis (Tables 2 and 3), it was observed that the structure of compound **9** was highly similar to the structure of elfvingic acid A,[14] except for the configuration of the double bond between C-20 and C-22. The correlation of H_3-21/H_2-24 observed by ROESY analysis (Figure S2-4) strongly suggested that the $\Delta^{20,22}$ was an *E*-configuration. The remaining location and relative stereochemistry of functions were determined to be the same as those of elfvingic acid A, while the absolute configuration of compound **9** (except for intractable C-25) was confirmed by comparison of the calculated and experimental ECD curves (Figure S2-5). Therefore, compound **9** was established as 12α,15β-dihydroxy-3,7,11,23-tetraoxolanosta-8,20*E*(22)-dien-26-oic acid (named gibbosic acid I).

Based on the NMR data analysis (Tables 2 and 3), the structure of compound **10** was found to be close to that of compound **9**, except for the presence of an oxygenated methine ($\delta_{H\text{-}11}$ 5.14, $\delta_{C\text{-}11}$ 77.4) in compound **10** vs a conjugated ketone group in **9**. Detailed analysis of 2D NMR correlations (Figure S2-6) found the key ^{1}H−^{1}H COSY correlation of H-11/H-12 and HMBC correlation of H-11 with C-8/C-13, which indicated that an OH group was located at C-11. The relative configuration of OH-11 was assigned β-orientation, based on the ROESY effects between H-11 and H_2-1. The absolute configuration of compound **10** (except for C-25) was confirmed by computational ECD (Figure S2-7), and the structure was determined to be 11β,12α,15β-trihydroxy-3,7,23-trioxolanosta-8,20*E*(22)-dien-26-oic acid (named gibbosic acid J).

Compound **11** was found to be similar to compound **9** based on NMR data analysis, except for an aliphatic methane

DOI: 10.1021/acs.jnatprod.9b00148
J. Nat. Prod. XXXX, XXX, XXX−XXX

Table 3. ^{1}H NMR Data for Compounds 9−15 (δ in ppm, J in Hz)

position	9[a]	10[b]	11[a]	12[a]	13[a]	14[c]	15[c]
1a	2.80, ddd (13.7, 7.7, 6.0)	3.17, overlap	2.21, overlap	2.20, overlap	2.25, overlap	1.99, m	2.17, overlap
1b	1.96, m	2.01, td (13.0, 4.6)	1.87, td (13.1, 5.5)	1.91, overlap	1.94, dd (18.8, 11.8)	1.65, overlap	1.73, overlap
2a	2.58, overlap	2.82, overlap	2.76, ddd (15.3, 13.3, 6.2)	2,26, overlap	2.72, overlap	2.80, td (14.8, 5.3)	2.80, td (14.4, 5.6)
2b	2.58, overlap	2.37, dt (15.2, 3.9)	2.46, overlap	2,26, overlap	2.58, overlap	2.30, dt (14.7, 3.3)	2.41, dq (15.2, 3.2)
5	2.33, dd (15.0, 2.3)	2.30, dd (14.2,3.6)	2.18, overlap	2.24, dd (14.6, 2.9)	2.23, overlap	1.63, overlap	1.73, dd, (12.0, 3.2)
6a	2.66, t (15.1)	2.85, overlap	2.65, overlap	2.62, overlap	2.66, overlap	2.04, t (6.4)	2.17, overlap
6b	2.51, overlap	2.62, dd (17.2, 3.6)	2.51, overlap	2.44, dd (16.0, 2.9)	2.53, overlap	1.95, t (5.6)	2.13, overlap
7						4.27, d (6.2)	6.92, d (8.0)
11a		5.14, overlap	2.94, overlap	6.12, d (9.9)	6.17, d (9.9)	6.57, s	5.88, s
11b			2.53, overlap				
12	3.72, s	4.43, s	3.83, d (7.1)	6.57, d (9.8)	6.62, d (9.8)		
15	4.43, d (7.4)	4.84, br s	4.38, d (7.0)	4.52, dd (9.3, 6.6)	4.47, d (7.2)	4.93, overlap	4.98, t (8.0)
16a	2.40, dt (16.5, 8.4)	2.56, overlap	2.42, overlap	2.50, m	2.47, m	2.60, overlap	2.73, overlap
16b	2.07, dd (14.1, 10.2)	2.56, overlap	2.21, overlap	1.92, overlap	2.22, overlap	2.10, overlap	2.26, ddd (13.6, 11.2, 7.2)
17	3.28, t (9.5)	3.66, t (9.5)	3.17, t (9.5)	2.99, overlap	2.78, overlap	3.50, dd (11.0, 7.2)	3.60, dd (10.4, 7.2)
18	1.28, s	1.70, s	1.35, s	0.78, s	1.29, s	1.33, s	1.07, s
19	0.90, s	1.60, s	0.78, s	1.22, overlap	1.02, s	0.39, s	1.22, s
21	2.20, s	2.58, s	2.25, s	2.21, s	2.27, s	2.58, s	2.64, s
22	6.29, s	6.75, s	6.32, s	6.17, s	6.27, s	6.07, s	6.79, s
24a	2.89, overlap	3.13, overlap	2.91, overlap	2.93, overlap	2.96, overlap	3.25, dd (17.1, 8.0)	3.29, dd (17.6, 8)
24b	2.54, overlap	2.57, overlap	2.62, overlap	2.61, overlap	2.63, overlap	2.70, dd (17.1, 5.6)	2.73, dd (17.6, 5.6)
25	2.94, overlap	3.28, m	2.96, overlap	2.91, overlap	2.98, overlap	3.33, dt (14.4, 7.3)	3.38, q (6.4)
27	1.19, d (6.8)	1.32, d (7.1)	1.23, d (6.9)	1.23, overlap	1.25, d (6.6)	1.37, d (7.2)	1.39, d (6.4)
28	1.13, s	1.11, s	1.12, overlap	1.14, s	1.15, s	1.11, s	1.12, s
29	1.10, s	1.06, s	1.15, overlap	1.13, s	1.16, s	0.96, s	1.06, s
30	1.26, s	1.52, s	1.10, overlap	1.10, s	0.97, s	1.34, s	1.48, s

[a]Measured at 600 MHz in chloroform-d. [b]Measured at 600 MHz in pyridine-d_5. [c]Measured at 800 MHz in pyridine-d_5.

in compound **11** replacing a conjugated ketone group in compound **9** and the methane group located at C-11, based on the correlation of H_2-11/H-12 in ^{1}H−^{1}H COSY spectra (Figure S2-8). All other functions and relative configurations were identical to those of compound **9**. With the exception of C-25, the absolute configuration of compound **11** was confirmed by ECD curve analysis (Figure S2-9). Therefore, compound **11** was assigned as 12α,15β-dihydroxy-3,7,23-trioxolanosta-8,20E(22)-dien-26-oic acid (named gibbosic acid K).

HRMS analysis established the same molecular formula ($C_{30}H_{40}O_6$) for compounds **12** and **13**. Comparison of their differences in NMR data (Tables 2 and 3) suggested that they were a pair of epimers with different configurations at C-15, like those of **2** and **4**. It was found there was a double bond in both **12** and **13** instead of an aliphatic methylene and an oxygenated methine as found in **11**. The double bonds in **12** and **13** were located between C-11 and C-12 according to HMBC correlations (Figure S2-10) of H-12 with C-9 and C-14, as well as of H_3-18 with C-12. All other functional groups and relative configurations were fully established from detailed 2D NMR analysis (Figures S2-10 and S2-11). The absolute configurations were confirmed by ECD curve analysis (Figures S2-12 and S2-13) (except for C-25), and the compounds were assigned as 15α-hydroxy-3,7,23-trioxolanosta-8,11,20E(22)-trien-26-oic acid (named gibbosic acid L) (**12**) and 15β-hydroxy-3,7,23-trioxolanosta-8,11,20E(22)-trien-26-oic acid (named gibbosic acid M) (**13**).

Compound **14** was found to be similar to the known compound applanoxidic acid A (**16**)[15] based on NMR data (Tables 2 and 3), except for distinct differences in the oxygenated region ($\delta_{C\text{-}7}$ 57.8, $\delta_{C\text{-}8}$ 62.4 in **14**; $\delta_{C\text{-}7}$ 60.5, $\delta_{C\text{-}8}$ 66.5 in **16**). From ROESY analyses (Figure S2-14), the correction of H-7 with H-30 indicated that H-7 was in an α-orientation and that the epoxy group was in a β-configuration. All other parts of compound **14** were found to be identical to the known compound **16**, according to detailed 2D NMR analyses (Figure S2-14). The absolute configuration of compound **14** was also assigned through comparing the calculated and experimental ECD curves (Figure S2-15). Therefore, the structure of compound **14** was established as 15α-hydroxy-7β,8β-epoxy-3,12,23-trioxolanosta-9(11),20E(22)-dien-26-oic acid (named gibbosic acid N).

NMR data showed (Tables 2 and 3) that compound **15** was similar to compound **14**, expect for an extra double-bond signal in **15** replacing two oxygenated carbon signals in **14**

DOI: 10.1021/acs.jnatprod.9b00148
J. Nat. Prod. XXXX, XXX, XXX−XXX

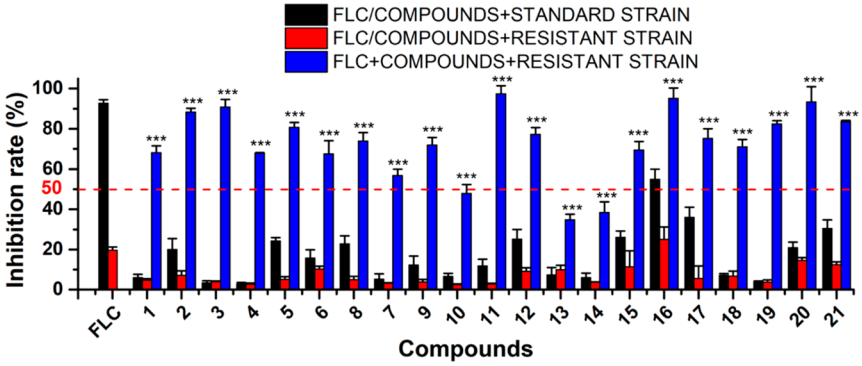

Figure 7. Inhibition rates of compounds **1**–**21** at 200 μg/mL, alone or in combination with FLC, against standard or FLC-resistant *C. albicans*. Inhibition was evaluated by the microbroth dilution assay, with FLC as the positive control for inhibition of both standard and FLC-resistant *C. albicans*. Each value is expressed as mean ± SD, (*) $p < 0.05$, (**) $p < 0.01$, and (***) $p < 0.001$ compared with the control ($n = 3$).

between C-7 and C-8. HMBC correlations (Figure S2-16) of H-7 with C-5, C-9, and C-14, as well as ^{1}H–^{1}H COSY correlations of H-5/H$_2$-6/H-7, indicate that the double bond was located between C-7 and C-8. Therefore, the structure of compound **15** was established as 15α-hydroxy-3,12,23-trioxolanosta-7,9(11),20*E*(22)-trien-26-oic acid (named gibbosic acid O).

Based on the plausible biogenetic considerations of the (23→26)-γ-lactone segment in compounds **2**–**8** (Scheme S3-1), the absolute configurations of which were identified with a high degree of confidence, the configurations at C-25 in compounds **9**–**15** could be safely assigned as *S*-configuration.

In the field of natural product research, X-ray single-crystal diffraction is currently considered to be the most reliable method for assigning absolute configurations of complex natural products. However, with the development of quantum chemistry calculations, computational methods (NMR, ECD, and optical rotatory dispersion (ORD)) have become increasingly common for structure elucidation of novel natural products.[16] Furthermore, recently some erroneous structures and spatial configurations previously reported have been revised using these methods.[17] In the present study, calculated chemical shifts with DP4+ analysis were preferred for establishing the stereochemistry of these new compounds. However, some configurations assigned from DP4+ possibility analysis were different from the above-elucidated stereochemistry. As shown in Table S1-1, the results of DP4+ analysis for assigning the configurations of 25*S**-**1** (100%), 25*S**-**2** (97%), 25*S**-**4** (100%), and 25*S**-**10** (99%) corresponded with the configurations (25*S*) established by the combination of calculated coupling constant and ECD. However, the configurations of 25*R**-**3** (97%), 25*R**-**5** (100%), and 25*R**-**9** (98%) assigned by DP4+ possibility analysis were notably contradictory to the configuration assignments above. In addition, the stereochemistry of 8-*epi*-cryptomoscatone D1 and isomers of maurenone, as part of the training set for DP4+ analysis, were also not satisfactorily assigned by DP4+ analysis even with the best computational level.[9] These compounds assigned in error by DP4+ analysis possess a similar characteristic: some independent and free-rotational stereoclusters. Accordingly, the DP4+ method could not be used with confidence to assign the configuration for these molecules, even with more than 97% DP4+ possibility, as in the cases of compounds **3**, **5**, and **9** in the present study. Although the DP4+ method can reliably establish configurations for most rigid organic molecules,[9,18] combinations of multiple methods are still suggested to accurately assign stereochemical configurations for flexible compounds.

The known compounds gibbosic acids A–C (**17**–**19**) from *G. gibbosum* were initially reported by our group.[6b] Other compounds identified were applanoxidic acid A (**16**),[15] elfvingic acid B (**20**),[14] and elfvingic acid C (**21**),[14] by comparing their spectroscopic data with those of previously published values. Compared to the new structures, there was an important difference: a double bond with an *E*-configuration between C-20 and C-22 in the all new compounds reported here vs a 20*S* hydroxy group in the known compounds.

The isolated metabolites were preliminarily evaluated for bioactivity at 200 μg/mL, alone or in combination with FLC, against standard or FLC-resistant *C. albicans* strains. Results (Figure 7, black and red columns) show that at 200 μg/mL concentrations these triterpenoid derivatives (except compound **16**, with a 55% inhibition rate against standard *C. albicans*) are not antifungal against standard and FLC-resistant *C. albicans* (inhibition rate <50%). The combination of these compounds with FLC at 200 μg/mL induced significant inhibitory antifungal activity against FLC-resistant *C. albicans* (Figure 7, blue column), suggesting that these compounds have a strong capacity to increase the susceptibility of FLC-resistant *C. albicans* to FLC. In concentration-dependent experiments, MIC$_{50}$ values were established for the combination of these compounds and FLC (Table 4), except for compounds **10**, **13**, and **14** (inhibition rate <50% at 200 μg/

Table 4. Antifungal Activities (MIC$_{50}$ Values = Mean ± SD, μg/mL) for Compounds and FLC in Combination (Ratio 1:1, μg/mL) against FLC-Resistant *C. albicans*[a]

compd	MIC$_{50}$	compd	MIC$_{50}$
1	78.0 ± 6.4	**12**	5.1 ± 1.6
2	4.7 ± 1.2	**15**	70.0 ± 11.2
3	47.9 ± 3.8	**16**	7.3 ± 2.4
4	37.8 ± 1.3	**17**	3.8 ± 1.1
5	5.0 ± 1.4	**18**	28.3 ± 4.7
6	29.4 ± 2.6	**19**	37.7 ± 1.7
7	25.8 ± 4.2	**20**	29.0 ± 2.6
8	129.1 ± 5.1	**21**	8.8 ± 1.6
9	4.4 ± 1.3		

[a]FLC against standard *C. albicans* was the positive control with MIC$_{50}$ 6.3 ± 1.2 μg/mL.

DOI: 10.1021/acs.jnatprod.9b00148
J. Nat. Prod. XXXX, XXX, XXX–XXX

mL). Results show that compounds **2**, **5**, **9**, **12**, **16**, **17**, and **21** exhibited strong antifungal activity in combination with FLC against resistant *C. albicans*, with MIC_{50} values ranging from 3.8 to 8.8 μg/mL, which are comparable to the MIC_{50} for FLC against standard *C. albicans*, of 6.3 μg/mL. Compounds **3**, **4**, **6**, **7**, **18**, **19**, and **20** had moderate effects in combination with FLC against resistant *C. albicans*, with MIC_{50} values ranging from 25.8 to 47.9 μg/mL.

EXPERIMENTAL SECTION

General Experimental Procedures. UV spectra were recorded using a Shimadzu UV-2401PC spectrophotometer. Optical rotations were obtained using a JASCO P-1020 digital polarimeter. CD spectra were recorded on an Applied Photophysics Chirascan circular dichroism spectrometer. IR spectra were measured on a Tenor 27 spectrophotometer with KBr pellets. All NMR spectra were established using a Bruker DRX-600 (or 800) spectrometer. Chemical shifts (δ) were expressed in parts per million with reference to the solvent signals. HRESIMS was performed using an Agilent G6230 TOF MS. Semipreparative HPLC was performed using an Agilent 1260 liquid chromatograph with a Zorbax SB-C_{18} (9.4 mm × 25 cm) column. Column chromatography (CC) was performed on silica gel (100−200 and 200−300 mesh; Qingdao Marine Chemical Inc., Qingdao, China), Lichroprep RP-18 gel (40−63 μm, Merck, Darmstadt, Germany), and Sephadex LH-20 (20−150 μm, Pharmacia). Fractions were monitored by TLC, with spots visualized under UV light (254 nm) and sprayed with 8% H_2SO_4 in ethanol, followed by heating.

Fungal Materials. The fruiting bodies of *Ganoderma gibbosum* were collected from Kunming city, China, in July 2015. A voucher specimen (Xiaowl 20150714) was deposited in the Herbarium of the School of Chemical Science and Technology, Yunnan University (China), and the specimen was identified by Dr. Zai-Wei Ge, Kunming Institute of Botany (China). The *C. albicans* strains, including FLC-resistant (SC5314) strain and FLC-susceptible strain (standard, ATCC 10231), were isolated from clinical patients and were generously provided by Dr. Yu-Ye Li, at the Hospital of Kunming Medical University (China).

Extraction and Isolation. Air-dried and powdered fruiting bodies of *G. gibbosum* (0.7 kg) were extracted in 3 L of 70% aqueous acetone for 48 h at room temperature and then filtered. This was repeated four times. Then the filtrate was evaporated under reduced pressure at 40 °C and partitioned between EtOAc and H_2O. The EtOAc-soluble portion (63 g) was fractionated by RP-18 gel CC (5 cm × 45 cm) and eluted using a CH_3OH−H_2O gradient system (30%, 60%, 90%, 100%), to produce fractions A−E.

Fraction B (5 g) was subjected to Sephadex LH-20 CC (3.5 cm × 180 cm, eluted with MeOH) extraction to remove red pigments, then purified by RP-18 gel CC (2.5 cm × 30 cm, MeOH−H_2O gradient, 30−100%) to give fractions B1−B8. The B2 fraction (50 mg) was purified by semipreparative HPLC (3 mL/min, detector UV λ_{max} 210, 254, and 280 nm, MeCN−H_2O, 42:58) to isolate compounds **9** (14.6 mg, 15.1 min) and **10** (5.2 mg, 13.5 min). Compound **20** (1.2 g) was crystallized from fraction B3 (2.5 g). The remaining part of fraction B3 was fractionated by silica gel CC (200−300 mesh) and eluted with $CHCl_3$−MeOH (gradient system: 50:1−10:1) to yielded fractions B3.1−B3.5. Then fraction B3.2 was purified by silica gel CC and semipreparative HPLC (mobile phase: MeCN−H_2O, 41:59) to yield compounds **14** (2.5 mg, 17.3 min) and **16** (10.7 mg, 16.5 min). The B3.4 fraction was subjected to semipreparative HPLC (mobile phase: MeCN−H_2O, 43:57) to yield compounds **17** (80.3 mg, 11.2 min), **18** (15.0 mg, 12.7 min), and **19** (25.1 mg, 15.6 min). B4 (0.3 g) was purified using silica gel CC and semipreparative HPLC (mobile phase: MeCN−H_2O, 44:56) to yield compounds **21** (15.1 mg, 9.5 min) and **15** (1.4 mg, 12.5 min). Fraction B5 (0.8 g) was fragmented using silica gel CC ($CHCl_3$−MeOH, 20:1) to obtain fractions B5.1−B5.3. Fraction B5.3 was purified by the same semipreparative HPLC system (mobile phase: MeCN−H_2O, 44:56) to afford compounds **11** (12.4 mg, 13.2 min), **12** (6.2 mg, 17.6 min), and **13** (8.7 mg, 14.5 min). Compounds **6** (16.7 mg, 17.4 min), **7** (12.3 mg, 19.0 min), and **8** (8.9 mg, 22.5 min) were obtained from fraction B6 (150 mg) by semipreparative HPLC (mobile phase: MeCN−H_2O, 41:59). Fraction B7 (230 mg) was further separated by a silica gel CC (mobile phase: petroleum ether−EtOAc, 4:1) to yield three fractions, B7.1−B7.3. B7.2 was purified by semipreparative HPLC (mobile phase: MeCN−H_2O, 46:54) to isolate compounds **2** (10.5 mg, 12.6 min) and **3** (7.2 mg, 13.5 min). Fraction B7.3 was purified by semipreparative HPLC (mobile phase: MeCN−H_2O, 45:55) to yield compounds **4** (13.4 mg, 14.0 min) and **5** (5.6 mg, 15.3 min). Fraction B8 (0.6 g) was subjected to silica gel CC (mobile phase: petroleum ether−EtOAc, 5:1) to isolate three fractions, B8.1−B8.3; then compound **1** (4.7 mg, 17.2 min) was separated from fraction B8.2 by semipreparative HPLC (mobile phase: MeCN−H_2O, 45:55).

*Ganoapplanilactones A (**1**):* white powder (MeOH); $[\alpha]^{21}_D$ −2.3 (*c* 0.07, MeOH); UV (MeOH) λ_{max} (log ε) 204 (3.99), 249 (3.76) nm; IR (KBr) ν_{max} 3441, 1707, 1383 cm^{-1}; ^1H and ^{13}C NMR data, see Figures S2-1 and S2-2; positive-ion ESIMS *m/z* 549 $[M + Na]^+$; positive-ion HRESIMS $[M + Na]^+$ *m/z* 549.2465 (calcd for 549.2464).

*Gibbosicolid A (**2**):* colorless solid; $[\alpha]^{21}_D$ +143.3 (*c* 0.09, MeOH); UV (MeOH) λ_{max} (log ε) 204 (4.05), 250 (3.99) nm; IR (KBr) ν_{max} 3442, 1685, 1186 cm^{-1}; ^1H and ^{13}C NMR data, see Tables 1 and 2; positive-ion ESIMS *m/z* 519 $[M + Na]^+$; positive-ion HRESIMS $[M + Na]^+$ *m/z* 519.2720 (calcd for 519.2723).

*Gibbosicolid B (**3**):* colorless solid; $[\alpha]^{21}_D$ +149.4 (*c* 0.09, MeOH); UV (MeOH) λ_{max} (log ε) 203 (4.12), 250 (4.10) nm; IR (KBr) ν_{max} 3442, 1685, 1198 cm^{-1}; ^1H and ^{13}C NMR data, see Tables 1 and 2; positive-ion ESIMS *m/z* 519 $[M + Na]^+$; positive-ion HRESIMS $[M + Na]^+$ *m/z* 519.2718 (calcd for 519.2723).

*Gibbosicolid C (**4**):* colorless solid; $[\alpha]^{21}_D$ +95.3 (*c* 0.08, MeOH); UV (MeOH) λ_{max} (log ε) 204 (4.05), 251 (3.97) nm; IR (KBr) ν_{max} 3441, 1683, 1188 cm^{-1}; ^1H and ^{13}C NMR data, see Tables 1 and 2; positive-ion ESIMS *m/z* 519 $[M + Na]^+$; positive-ion HRESIMS $[M + Na]^+$ *m/z* 519.2720 (calcd for 519.2723).

*Gibbosicolid D (**5**):* colorless solid; $[\alpha]^{21}_D$ +93.4 (*c* 0.10, MeOH); UV (MeOH) λ_{max} (log ε) 203 (4.12), 251 (4.10) nm; IR (KBr) ν_{max} 3444, 1683, 1198 cm^{-1}; ^1H and ^{13}C NMR data, see Tables 1 and 2; positive-ion ESIMS *m/z* 519 $[M + Na]^+$; positive-ion HRESIMS $[M + Na]^+$ *m/z* 519.2722 (calcd for 519.2723).

*Gibbosicolid E (**6**):* white powder; $[\alpha]^{21}_D$ +129.4 (*c* 0.10, MeOH); UV (MeOH) λ_{max} (log ε) 203 (4.25), 249 (4.16) nm; IR (KBr) ν_{max} 3432, 1683, 1195 cm^{-1}; ^1H and ^{13}C NMR data, see Tables 1 and 2; positive-ion ESIMS *m/z* 535 $[M + Na]^+$; positive-ion HRESIMS $[M + Na]^+$ *m/z* 535.2665 (calcd for 535.2672).

*Gibbosicolid F (**7**):* white powder; $[\alpha]^{21}_D$ +70.7 (*c* 0.09, MeOH); UV (MeOH) λ_{max} (log ε) 204 (4.11), 251 (4.00) nm; IR (KBr) ν_{max} 3435, 1681, 1197 cm^{-1}; ^1H and ^{13}C NMR data, see Tables 1 and 2; positive-ion ESIMS *m/z* 535 $[M + Na]^+$; positive-ion HRESIMS $[M + Na]^+$ *m/z* 535.2668 (calcd for 535.2672).

*Gibbosicolid G (**8**):* white powder; $[\alpha]^{19}_D$ +88.3 (*c* 0.10, MeOH); UV (MeOH) λ_{max} (log ε) 203 (4.09), 249 (4.02) nm; IR (KBr) ν_{max} 3430, 1738, 1683, 1198 cm^{-1}; ^1H and ^{13}C NMR data, see Tables 1 and 2; positive-ion ESIMS *m/z* 549 $[M + Na]^+$; positive-ion HRESIMS $[M + Na]^+$ *m/z* 549.2822 (calcd for 549.2828).

*Gibbosic acid I (**9**):* white powder; (MeOH); $[\alpha]^{21}_D$ +40.7 (*c* 0.15, MeOH); UV (MeOH) λ_{max} (log ε) 248 (4.06) nm; IR (KBr) ν_{max} 3432, 2975, 1710, 1385 cm^{-1}; ^1H and ^{13}C NMR data, see Tables 2 and 3; negative-ion ESIMS *m/z* 527 $[M - H]^-$; positive-ion HRESIMS $[M + Na]^+$ *m/z* 551.2612 (calcd for 551.2621).

*Gibbosic acid J (**10**):* white, microcrystalline solid (MeOH); $[\alpha]^{21}_D$ −11.9 (*c* 0.09, MeOH); UV (MeOH) λ_{max} (log ε) 240 (4.21) nm; IR (KBr) ν_{max} 3434, 1712, 1381 cm^{-1}; ^1H and ^{13}C NMR data, see Tables 2 and 3; negative-ion ESIMS *m/z* 529 $[M - H]^-$; positive-ion HRESIMS $[M + Na]^+$ *m/z* 553.2772 (calcd for 553.2777).

*Gibbosic acid K (**11**):* white powder; $[\alpha]^{19}_D$ −42.9 (*c* 0.10, MeOH); UV (MeOH) λ_{max} (log ε) 248 (4.18) nm; IR (KBr) ν_{max} 3437, 1708, 1382 cm^{-1}; ^1H and ^{13}C NMR data, see Tables 2 and 3; positive-ion ESIMS *m/z* 537 $[M + Na]^+$; positive-ion HRESIMS $[M + Na]^+$ *m/z* 537.2821 (calcd for 537.2828).

DOI: 10.1021/acs.jnatprod.9b00148
J. Nat. Prod. XXXX, XXX, XXX−XXX

Gibbosic acid L (12): yellowish powder; $[\alpha]^{21}_{D}$ −45.1 (*c* 0.10, MeOH); UV (MeOH) λ_{max} (log ε) 242 (4.04), 315 (3.64) nm; IR (KBr) ν_{max} 3437, 1708, 1640 cm^{-1}; ^{1}H and ^{13}C NMR data, see Tables 2 and 3; positive-ion ESIMS *m/z* 519 $[M + Na]^+$; positive-ion HRESIMS $[M + Na]^+$ *m/z* 519.2722 (calcd for 519.2723).

Gibbosic acid M (13): yellowish powder; $[\alpha]^{19}_{D}$ −141.0 (*c* 0.18, MeOH); UV (MeOH) λ_{max} (log ε) 245 (4.14), 317 (3.64) nm; IR (KBr) ν_{max} 3431, 1708, 1383 cm^{-1}; ^{1}H and ^{13}C NMR data, see Tables 2 and 3; positive-ion ESIMS *m/z* 519 $[M + Na]^+$; positive-ion HRESIMS $[M + Na]^+$ *m/z* 519.2721 (calcd for 519.2723).

Gibbosic acid N (14): white powder; $[\alpha]^{21}_{D}$ +114.2 (*c* 0.08, MeOH); UV (MeOH) λ_{max} (log ε) 247 (4.27); IR (KBr) ν_{max} 3435, 2978, 1686, 1385 cm^{-1}; ^{1}H and ^{13}C NMR data, see Tables 2 and 3; negative-ion ESIMS *m/z* 511 $[M - H]^-$; positive-ion HRESIMS $[M + Na]^+$ *m/z* 535.2673 (calcd for 535.2672).

Gibbosic acid O (15): yellowish powder; $[\alpha]^{21}_{D}$ −17.0 (*c* 0.10, MeOH); UV (MeOH) λ_{max} (log ε) 201 (3.80), 254 (3.86); IR (KBr) ν_{max} 3448, 1619, 1400 cm^{-1}; ^{1}H and ^{13}C NMR data, see Tables 2 and 3; negative-ion ESIMS *m/z* 495 $[M - H]^-$; positive-ion HRESIMS $[M + Na]^+$ *m/z* 519.2720 (calcd for 519.2723).

Quantum Chemistry Calculations. All theoretical calculations were carried out using the Gaussian 09 program package.[19] Conformation search by MMFF94S molecular force fields was performed for all possible isomers, providing corresponding stable conformers with distributions higher than 1%.[20] The conformers were optimized using the DFT method at the B3LYP/6-31+G(d,p) level in chloroform, using the PCM model for NMR (or in methanol, using the PCM model for ECD). Then further conformer analyses were performed according to the frequency and Boltzmann distribution theory to remove unreasonable and unstable conformers, while room-temperature equilibrium proportions were calculated according to the Boltzmann distribution law.

GIAO calculations[12] of NMR shielding constants with spin−spin interactions were accomplished for all stable conformers using the DFT method at the mPW1PW91/6-311G(d,p) level in chloroform or pyridine, using the PCM model. The shielding constants (including ^{13}C and ^{1}H) obtained were directly statistically analyzed with experimental chemical shifts, using DP4+ probability.[9] The calculated coupling constants of these conformers were averaged according to the Boltzmann distribution theory and their relative Gibbs free energy.

The theoretically calculated ECD spectra were established using the TDDFT method[13] at the B3LYP/6-311+G(d,p) level in methanol, using the PCM model, including in all cases 30 excited states. The ECD spectra were simulated by SpecDis[21] (version 1.64) using σ = 0.15−0.30 eV and $R^{velocity}$. All calculated curves were shifted from −15 to +15 nm to better simulate experimental spectra. The predicted ECD spectra of enantiomers were simulated directly using SpecDis software.

Orbital information (NBO plot files) was generated using the NBO program of Gaussian 09 at the B3LYP/6-311+G(d,p) level in MeOH, using the PCM model. The predominantly populated conformers were selected for molecular orbital analysis. NBO and transition density plots were generated by Gaussian outputs using Multiwfn 3.4[22] and VMD software packages.[23]

Antifungal Activity Assay. A 200 μg/mL concentration of each compound and FLC alone or in combination (ratio 1:1, μg/mL) were assessed against standard or FLC-resistant *C. albicans*, to screen antifungal activity. Compounds with inhibition ratios of more than 50% were selected to establish the minimal concentration of 50% inhibition (MIC_{50}) against *C. albicans* strains. The MIC_{50} was tested using a microbroth dilution assay in 96-well microplates. Briefly, 100 μL of *C. albicans* (1 × 105) and 100 μL of antifungal solutions were added in triplicate to 96-well flat plates. The concentrations of fluconazole and test compounds were diluted 5-fold, from 200 to 0.32 μg/mL. Fluconazole was used as a positive control with definite activity against FLC-susceptible *C. albicans*. In addition, blank control wells were used without antifungal solution, and the medium-only cultures were used to establish the background. After incubation at 37 °C for 24 h, absorbance was measured at 625 nm.

■ ASSOCIATED CONTENT

Supporting Information

The Supporting Information is available free of charge on the ACS Publications website at DOI: 10.1021/acs.jnatprod.9b00148.

Results of DP4+ analysis for **1**−**5**, **9**, and **10**; important 2D correlations and ECD spectra for **9**−**15**; plausible biosynthetic pathway of lactone formation for **2**−**8**; detailed ^{1}D and ^{2}D NMR, HRESIMS, IR, and UV spectra for **1**−**15**; computational data of compounds **1**−**15** (PDF)

■ AUTHOR INFORMATION

Corresponding Authors

*E-mail: lixiaoli@ynu.edu.cn.
*E-mail: wangrr1980@163.com.
*E-mail: xiaoweilie@ynu.edu.cn.

ORCID

Debing Pu: 0000-0001-5514-304X
Weilie Xiao: 0000-0001-6826-1993

Author Contributions

⊥D.-B. Pu and X.-N. Li contributed equally to this work.

Notes

The authors declare no competing financial interest.

■ ACKNOWLEDGMENTS

This project was financially supported by the NSFC (81422046 and 21762048), the Postdoctoral Science Foundation of China (2018M633428), the Yunnan Science and Technology Planning Project (2017FF117), the Yunnan Applicative and Basic Research Program (2018FY001 and 2018FA004), the Project of Innovative Research Team of Yunnan Province to W.-L.X., and the Program for Changjiang Scholars and Innovative Research Team in University (IRT_17R94). All spectral data were recorded at the Analysis and Testing Center of Kunming Institute of Botany. The calculation resources were supported by the High-Performance Computing Center of Yunnan University. We are grateful to Dr. Z-W. Ge (Kunming Institute of Botany, China) for identifying the *G. gibbosum* specimen and Dr. Y.-Y. Li (Hospital of Kunming Medical University, China) for providing *C. albicans* strains.

■ REFERENCES

(1) Wellington, M.; Koselny, K.; Sutterwala, F. S.; Krysan, D. J. *Eukaryotic Cell* **2014**, *13*, 329−340.

(2) Delaloye, J.; Calandra, T. *Virulence* **2014**, *5*, 161−169.

(3) Shi, J.; Li, S.; Gao, A.; Zhu, K.; Zhang, H. *Phytomedicine* **2018**, *46*, 21−31.

(4) Andersson, D. I.; Hughes, D. *Nat. Rev. Microbiol.* **2010**, *8*, 260−271.

(5) (a) Zacchino, S. A.; Butassi, E.; Liberto, M. D.; Raimondi, M.; Postigo, A.; Sortino, M. *Phytomedicine* **2017**, *37*, 27−48. (b) Okabe, M.; Sugita, T.; Kinoshita, K.; Koyama, K. *J. Nat. Prod.* **2016**, *79*, 1208−1212.

(6) (a) Peng, X. R.; Liu, J. Q.; Wang, C. F.; Li, X. Y.; Shu, Y.; Zhou, L.; Qiu, M. H. *J. Nat. Prod.* **2014**, *77*, 737−743. (b) Pu, D. B.; Zheng, X.; Gao, J. B.; Zhang, X. J.; Qi, Y.; Li, X. S.; Wang, Y. M.; Li, X. N.; Li, X. L.; Wan, C. P.; Xiao, W. L. *Fitoterapia* **2017**, *119*, 1−7.

(7) (a) Shiao, M. S. *Chem. Rec.* **2010**, *3*, 172−180. (b) Wu, J. G.; Kan, Y. J.; Wu, Y. B.; Yi, J.; Chen, T. Q.; Wu, J. Z. *Pharm. Biol.* **2016**, *54*, 919−929.

DOI: 10.1021/acs.jnatprod.9b00148
J. Nat. Prod. XXXX, XXX, XXX−XXX

(8) (a) Zhao, X. R.; Huo, X. K.; Dong, P. P.; Wang, C.; Huang, S. S.; Zhang, B. J.; Zhang, H. L.; Deng, S.; Liu, K. X.; Ma, X. C. *J. Nat. Prod.* **2015**, *78*, 1868−1876. (b) Jiao, Y.; Xie, T.; Zou, L. H.; Wei, Q.; Qiu, L.; Chen, L. X. *Bioorg. Med. Chem. Lett.* **2016**, *26*, 3556−3561.
(9) Grimblat, N.; Zanardi, M. M.; Sarotti, A. M. *J. Org. Chem.* **2015**, *80*, 12526−12534.
(10) Li, L.; Peng, X. R.; Dong, J. R.; Lu, S. Y.; Li, X. N.; Zhou, L.; Qiu, M. H. *RSC Adv.* **2018**, *8*, 31287−31295.
(11) León, F.; Valencia, M.; Rivera, A.; Nieto, I.; Quintana, J.; Estévez, F.; Bermejo, J. *Helv. Chim. Acta* **2010**, *86*, 3088−3095.
(12) Lodewyk, M. W.; Siebert, M. R.; Tantillo, D. J. *Chem. Rev.* **2012**, *112*, 1839−1862.
(13) Srebro-Hooper, M.; Autschbach, J. *Annu. Rev. Phys. Chem.* **2017**, *68*, 399−420.
(14) Yoshikawa, K.; Nishimura, N.; Bando, S.; Arihara, S.; Matsumura, E.; Katayama, S. *J. Nat. Prod.* **2002**, *65*, 548−552.
(15) Chairul; Tokuyama, T.; Hayashi, Y.; Nishizawa, M.; Tokuda, H.; Chairul, S. M.; Hayashi, Y. *Phytochemistry* **1991**, *30*, 4105−4109.
(16) (a) Menna, M.; Imperatore, C.; Mangoni, A.; Della Sala, G.; Taglialatela-Scafati, O. *Nat. Prod. Rep.* **2019**, *36*, 476. (b) Bifulco, G.; Dambruoso, P.; Gomez-Paloma, L.; Riccio, R. *Chem. Rev.* **2007**, *107*, 3744−3779.
(17) Chhetri, B. K.; Lavoie, S.; Sweeney-Jones, A. M.; Kubanek, J. *Nat. Prod. Rep.* **2018**, *35*, 514−531.
(18) (a) Wang, X.; Liu, J.; Pandey, P.; Fronczek, F. R.; Doerksen, R. J.; Chen, J.; Qi, X.; Zhang, P.; Ferreira, D.; Valeriote, F. A.; Sun, H.; Li, S.; Hamann, M. T. *Org. Lett.* **2018**, *20*, 5559−5563. (b) Pu, D. B.; Du, B. W.; Chen, W.; Gao, J. B.; Hu, K.; Shi, N.; Li, Y. M.; Zhang, X. J.; Zhang, R. H.; Li, X. N.; Zhang, H. B.; Wang, F.; Xiao, W. L. *Org. Lett.* **2018**, *20*, 6314−6317.
(19) Frisch, M. J.; Schlegel, H. B.; Scuseria, G. E.; Robb, M. A.; Cheeseman, J. R.; Scalmani, G.; Barone, V.; Mennucci, B.; Petersson, G. A.; Nakatsuji, H.; Caricato, M.; Li, X.; Hratchian, H. P.; Izmaylov, A. F.; Bloino, J.; Zheng, G.; Sonnenberg, J. L.; Hada, M.; Ehara, M.; Toyota, K.; Fukuda, R.; Hasegawa, J.; Ishida, M.; Nakajima, T.; Honda, Y.; Kitao, O.; Nakai, H.; Vreven, T.; Montgomery, J. A., Jr.; Ogliaro, F.; Bearpark, M.; Heyd, J. J.; Brothers, E.; Kudin, K. N.; Staroverov, V. N.; Keith, T.; Kobayashi, R.; Normand, J.; Raghavachari, K.; Rendell, A.; Burant, J. C.; Iyengar, S. S.; Tomasi, J.; Cossi, M.; Rega, N.; Millam, J. M.; Klene, M.; Knox, J. E.; Cross, J. B.; Bakken, V.; Adamo, C.; Jaramillo, J.; Gomperts, R.; Stratmann, R. E.; Yazyev, O.; Austin, A. J.; Cammi, R.; Pomelli, C.; Ochterski, J. W.; Martin, R. L.; Morokuma, K.; Zakrzewski, V. G.; Voth, G. A.; Salvador, P.; Dannenberg, J. J.; Dapprich, S.; Daniels, A. D.; Farkas, O.; Foresman, J. B.; Ortiz, J. V.; Cioslowski, J.; Fox, D. J. *Gaussian 09*, Revision C.01; Gaussian, Inc.: Wallingford, CT, 2010.
(20) Gotō, H.; Ōsawa, E. *J. Chem. Soc., Perkin Trans. 2* **1993**, *2*, 187−198.
(21) Bruhn, T. S. A.; Hemberger, Y. *Spec Dis*, Version 1.64; University of Wuerzburg, 2015.
(22) Lu, T.; Chen, F. *J. Comput. Chem.* **2012**, *33*, 580−592.
(23) Humphrey, W.; Dalke, A.; Schulten, K. *J. Mol. Graphics* **1996**, *14*, 33−38.

DOI: 10.1021/acs.jnatprod.9b00148
J. Nat. Prod. XXXX, XXX, XXX−XXX